

Ca²⁺-mediated activation of the skeletal-muscle ryanodine receptor ion channel

Received for publication, June 13, 2018, and in revised form, October 14, 2018. Published, Papers in Press, October 19, 2018, DOI 10.1074/jbc.RA118.004453

Le Xu[‡], Venkat R. Chirasani^{‡§}, Jordan S. Carter^{¶||}, Daniel A. Pasek[‡], Nikolay V. Dokholyan^{‡§}, Naohiro Yamaguchi^{¶||}, and Gerhard Meissner^{‡¶1}

From the [‡]Department of Biochemistry and Biophysics, University of North Carolina, Chapel Hill, North Carolina 27599-7260, the [§]Departments of Pharmacology and Biochemistry and Molecular Biology, Penn State College of Medicine, Hershey, Pennsylvania 17033-0850, the [¶]Department of Regenerative Medicine and Cell Biology, Medical University of South Carolina, Charleston, South Carolina 29425, and the ^{||}Cardiac Signaling Center, Clemson University, Charleston, South Carolina 29425

Edited by Mike Shipston

Cryo-electron micrograph studies recently have identified a Ca²⁺-binding site in the 2,200-kDa ryanodine receptor ion channel (RyR1) in skeletal muscle. To clarify the role of this site in regulating RyR1 activity, here we applied mutational, electrophysiological, and computational methods. Three amino acid residues that interact directly with Ca²⁺ were replaced, and these RyR1 variants were expressed in HEK293 cells. Single-site RyR1-E3893Q, -E3893V, -E3967Q, -E3967V, and -T5001A variants and double-site RyR1-E3893Q/E3967Q and -E3893V/E3967V variants displayed cellular Ca²⁺ release in response to caffeine, which indicated that they retained functionality as caffeine-sensitive, Ca²⁺-conducting channels in the HEK293 cell system. Using [³H]ryanodine binding and single-channel measurements of membrane isolates, we found that single- and double-site RyR1-E3893 and -E3967 variants are not activated by Ca²⁺. We also noted that RyR1-E3893Q/E3967Q and -E3893V/E3967V variants maintain caffeine- and ATP-induced activation and that RyR1-E3893Q/E3967Q is inhibited by Mg²⁺ and elevated Ca²⁺. RyR1-T5001A exhibited decreased Ca²⁺ sensitivity compared with WT-RyR1 in single-channel measurements. Computational methods suggested that electrostatic interactions between Ca²⁺ and negatively charged glutamate residues have a critical role in transducing the functional effects of Ca²⁺ on RyR1. We conclude that the removal of negative charges in the recently identified RyR1 Ca²⁺-binding site impairs RyR1 activation by physiological Ca²⁺ concentrations and results in loss of binding to Ca²⁺ or reduced Ca²⁺ affinity of the binding site.

Ryanodine receptor ion channels (RyRs)² release Ca²⁺ from intracellular Ca²⁺-storing compartments to regulate multiple cellular functions (1–4). There are three mammalian RyR iso-

forms. RyR1 is present in skeletal muscle, RyR2 is present in heart muscle, and RyR3 is present at low levels in many tissues, including brain and slow-twitch skeletal muscle. Calcium ions play a predominant role in the regulation of RyRs. Activation by micromolar Ca²⁺ and inhibition by millimolar Ca²⁺ suggest the presence of high-affinity Ca²⁺ activation and low-affinity Ca²⁺ inactivation sites. Additional regulation is mediated by ATP and caffeine, which increase Ca²⁺-gated RyR activities. Mg²⁺ inhibits Ca²⁺-activated RyRs by competing with Ca²⁺ for high-affinity Ca²⁺ activation sites and by binding to inhibitory low-affinity divalent cation sites (3).

Cryo-EM studies have provided detailed information about closed and open structures of the 2,200-kDa RyRs (5–12). Des Georges *et al.* (9) determined the location of RyR1-binding sites for endogenous channel activators Ca²⁺ and ATP and the exogenous activator caffeine (Fig. 1). Ca²⁺ or ATP/caffeine alone induced structural changes in the large cytosolic domain and primed RyR1 to nearly full open conformation in the presence of the three channel activators (9).

Three conserved amino acid residues contribute to the primary coordination sphere of bound Ca²⁺ in the large cytoplasmic domain of RyRs. Thr-5001 is conserved in RyRs, whereas RyR1 residues Glu-3893 and Glu-3967 are conserved in both RyRs and the related inositol trisphosphate receptor families. The RyRs and IP₃ receptors are expressed in intracellular membrane compartments containing up to millimolar concentrations of bound and free Ca²⁺. The release of Ca²⁺ is triggered by a Ca²⁺-induced Ca²⁺ release mechanism for the cardiac and brain RyR isoforms and by the action of IP₃ and Ca²⁺ for the IP₃ receptors (3, 13). A distinguishing feature of skeletal muscle is that voltage-sensing L-type Ca²⁺ channels (DHPRs, Cav1.1s) open juxtaposed RyR1s through direct protein–protein interactions (14). Ca²⁺-induced Ca²⁺ release is regulated on a slow time scale in mammalian skeletal muscle compared with physiological rates of Ca²⁺ release (15, 16). This suggests that while having a predominant role in the regulation of cardiac and brain RyR isoforms, Ca²⁺ may have a more confined role in the activation of mammalian skeletal-muscle RyRs.

The present study tested the hypothesis that the Ca²⁺-binding site identified by cryo-EM (9) has a major role in transducing the functional effects of Ca²⁺ in RyR1. Five single-site RyR1 variants (E3893Q, E3893V, E3967Q, E3967V, and T5001A) and two double-site RyR1 variants (E3893Q/E3967Q and E3893V/

This work was supported by National Institutes of Health Grants AR018687 (to G. M.) and P20GM103499 and UL1TR001450 (to N. Y.). The authors declare that they have no conflicts of interest with the contents of this article. The content is solely the responsibility of the authors and does not necessarily represent the official views of the National Institutes of Health.

¹To whom correspondence should be addressed: Dept. of Biochemistry and Biophysics, University of North Carolina, Chapel Hill, NC 27599-7260. Tel.: 919-966-5021; E-mail: meissner@med.unc.edu.

²The abbreviations used are: RyR, ryanodine receptor ion channel; FKBP, FK506-binding protein; ANOVA, analysis of variance; PDB, Protein Data Bank; IP₃, inositol 1,4,5-trisphosphate.

Activation of RyR1 by Ca²⁺

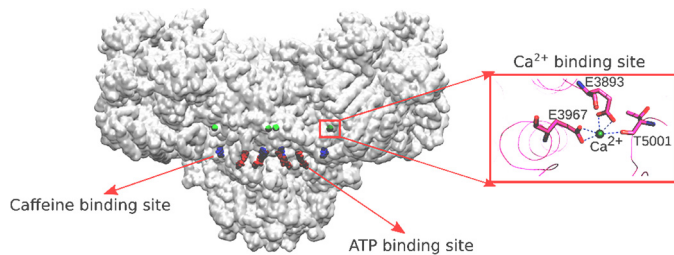


Figure 1. Location of Ca²⁺-, ATP-, and caffeine-binding sites of open RyR1 (PDB code 5TAL). The protein structure is shown as a transparent surface. Inset, structure of Ca²⁺-binding site of open RyR1 (PDB code 5TAL).

E3967V) were expressed as caffeine-sensitive, Ca²⁺-conducting channels in HEK293 cells. Studies using membrane isolates suggested that Ca²⁺ did not significantly activate single- and double-site RyR1-E3893 and -E3967 variants, whereas RyR1-T5001A exhibited altered Ca²⁺-dependent regulation compared with WT. Computational methods using cryo-EM micrograph densities provided structural information on the interaction between Ca²⁺ and amino acid residues of the Ca²⁺-binding sites of RyR1-WT and variant channels.

Results

Three conserved amino acid residues (Glu-3893, Glu-3967, and Thr-5001) were shown previously to directly interact with Ca²⁺ in a Ca²⁺-binding site in RyR1 (Fig. 1) (9). In the present study, we focused on the role of the two negatively charged glutamates in regulating RyR1 activity. Negative charges were removed by replacing one or both Glu residues with Gln or Val (RyR1-E3893Q, -E3893V, -E3967Q, -E3967V, -E3893Q/E3967Q, and -E3893V/E3967V) while maintaining residue volumes (17). RyR1 Thr-5001 was mutated to Ala, reducing the size of the side chain at this position. SDS-PAGE and immunoblot analysis indicated that single- and double-site RyR1-E3893 and -E3967 variants were expressed at variable, elevated levels compared with WT and RyR1-T5001A at a level comparable with WT (Fig. 2, top and Table 1).

The expression of functional RyR1 variant channels was monitored in HEK293 cells using the RyR1 agonist caffeine and fluorescence Ca²⁺ indicator Fluo-4. Millimolar caffeine activates RyR1 (18) and has little effect on Fluo-4 fluorescence in HEK293 cells transfected with the pCMV5 plasmid (Fig. 2, bottom). A variable caffeine-induced Ca²⁺ release was observed in 30–60% of HEK293 cells transfected with WT-RyR1. The variable response may have resulted from uneven exposure to caffeine and/or removal of released Ca²⁺ by HEK293 cellular transport systems. The number of variant HEK293 cells showing caffeine-induced Ca²⁺ release ranged from 46.5% for RyR1-E3967V to 119% for RyR1-E3893Q compared with WT (Table 1). These observations suggest that all variants expressed caffeine-sensitive, Ca²⁺-conducting channels in HEK293 cells.

Two methods were used to determine WT and variant activities. Regulation by Ca²⁺ was directly measured using the lipid bilayer method (19) (see below). In a second widely used but less direct method, Ca²⁺-dependent RyR activity was determined using the RyR-specific plant alkaloid ryanodine (20).

Specific [³H]ryanodine binding to WT showed a bimodal Ca²⁺ activation/Ca²⁺ inhibition profile with peak activity at

~70 μM Ca²⁺ (Fig. 3). [³H]Ryanodine binding to RyR1-T5001A was lower than WT. In contrast to RyR1-WT and -T5001A, RyR1-E3893 and -E3967 variants displayed the highest [³H]ryanodine binding levels at submicromolar Ca²⁺ (Fig. 3). RyR1-E3893Q/E3967Q bound the highest amount of [³H]ryanodine at <1 μM Ca²⁺ (~275 fmol/mg protein), followed by E3967Q and E3893Q (~55 and ~40 fmol/mg protein, respectively), E3893V (~20 fmol/mg protein), and E3967V and E3893V/E3967V variants (~11 and 15 fmol/mg protein, respectively). Elevated Ca²⁺ concentrations inhibited [³H]ryanodine binding for all variants, with IC₅₀ values ranging from 50 to 200 μM Ca²⁺.

We considered the possibility that the different [³H]ryanodine binding levels of the variants in Fig. 3 could be accounted for by varying levels of expression in HEK293 cells and/or recovery of functional variants in the membrane isolates. We assessed this in recording single channels using the lipid bilayer method, which directly compares WT and variant activities. RyR1s were recorded as K⁺-conducting channels using 0.25 M KCl on both sides of the bilayer at cytosolic Ca²⁺ ranging from 0.01 μM Ca²⁺ to 10 mM Ca²⁺.

RyR1-WT showed a biphasic Ca²⁺ activation/inhibition profile with a maximum averaged channel open probability (P_o) of 0.16 at ~20 μM cytosolic Ca²⁺ (Fig. 4). RyR1-T5001A resulted in a rightward shift of the P_o-Ca²⁺ activation response curve and reduced peak P_o at ~100 μM Ca²⁺ compared with WT at 20 μM Ca²⁺.

In agreement with the [³H]ryanodine-binding data of Fig. 3, RyR1-E3893Q/E3967Q was not significantly activated by Ca²⁺. Averaged P_o was 0.02 at 0.01 μM Ca²⁺ (Table 1) and half-maximal levels at ~6 μM Ca²⁺ (Fig. 4B) suggested that binding of elevated cytosolic Ca²⁺ had an inhibitory effect (p < 0.05). One possibility we could not rule out is that the presence of Ca²⁺-inhibitory sites interfered with the activation of RyR1-E3893Q/E3967Q by the binding of Ca²⁺ to low-affinity sites. RyR1-E3893Q, -E3893V, -E3967Q, -E3967V, and -E3893V/E3967V had very low averaged P_o values of 0.002 and less at Ca²⁺ ranging from 0.01 to 2 μM (Table 1). The results suggest that the two negatively charged Glu-3893 and Glu-3967 residues have a critical role in transducing the functional effects of Ca²⁺ in RyR1.

The amino acid mutations could have potentially modified the RyR1 ion permeation properties, resulting in reduced K⁺ conductances and loss of Ca²⁺ conductances (3). However, measurement of the voltage dependence of variant channel currents indicated that K⁺ conductances were similar to WT (Table 1). In the presence of 10 mM luminal Ca²⁺, RyR1-E3893Q/E3967Q and T5001A variants conducted Ca²⁺ and maintained a Ca²⁺/K⁺ permeability ratio similar to WT. The permeability ratio of the remaining variants could not be determined due to low open channel probabilities.

Des Georges *et al.* (9) determined single-channel activities of the purified RyR1-FK506-binding protein 12.6 (FKBP12.6, Calstabin2) complex reconstituted in lipid bilayer vesicles. FKBP12.6 and the related FKBP12 bind with nanomolar affinity to RyRs and are considered constitutive members of RyR ion channel complexes. Dissociation of FKBP12 from the homotetrameric RyR1 complex increased channel open probability and

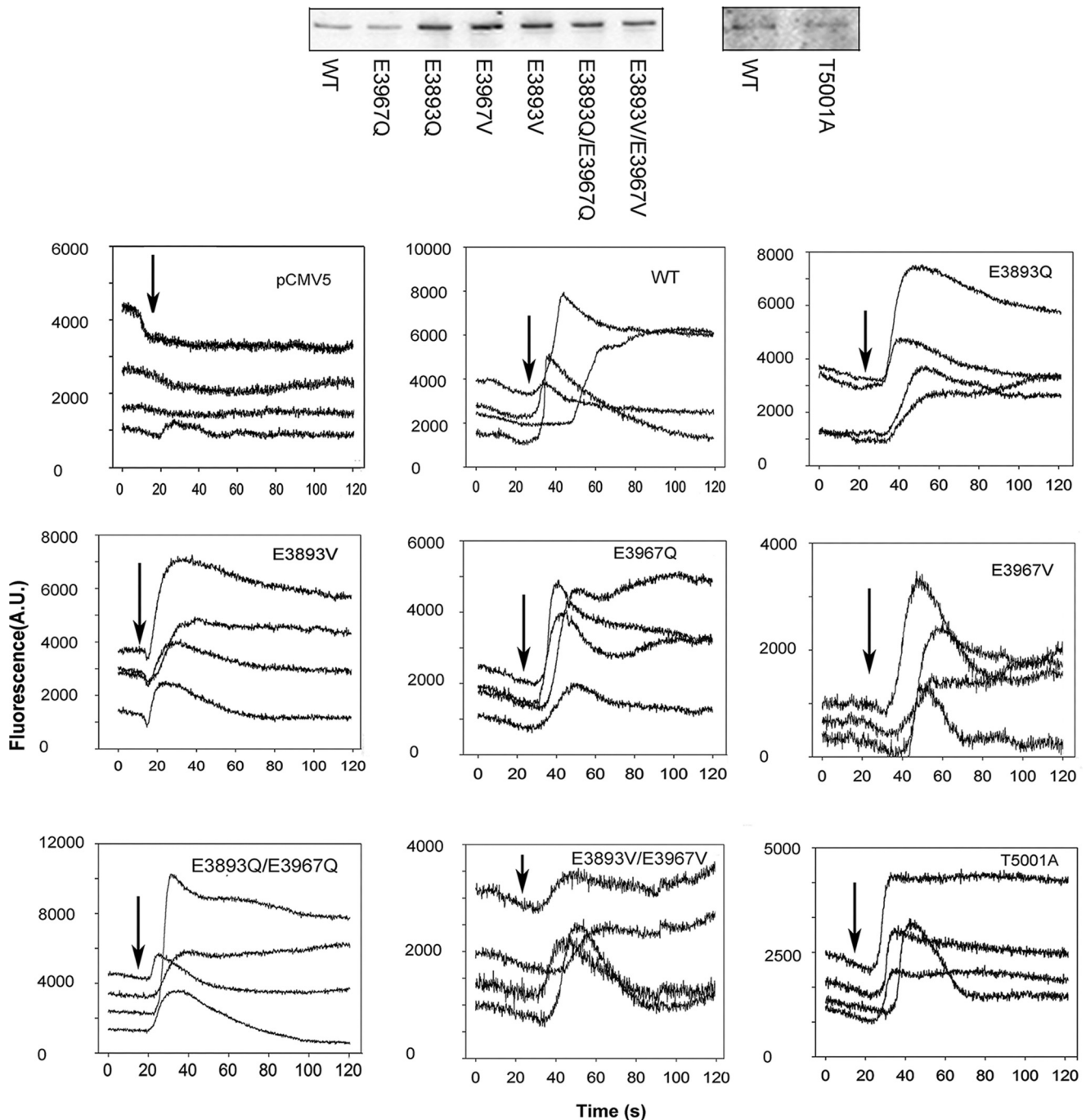


Figure 2. Immunoblots and caffeine-induced Ca^{2+} release in HEK293 cells transfected with WT and variant RyR1s. *Top*, proteins (20 $\mu\text{g}/\text{lane}$) were separated on 3–12% gradient SDS-PAGE, transferred to nitrocellulose membranes, and probed with primary rabbit anti-RyR1 antibody and peroxidase-conjugated anti-rabbit IgG. WT and variant 565-kDa RyR1 polypeptide bands are shown. *Bottom*, Ca^{2+} transients were determined in Ca^{2+} -free Krebs–Ringer–Henseleit bath solution as changes of Fluo-4 fluorescence before and after the addition of ~ 8 mM caffeine to the bath solution. *Arrows*, the position of caffeine addition to cells. Averaged data in Table 1 were corrected for number of pCMV5-transfected cells that showed a caffeine signal ($\sim 10\%$ of WT transfected cells). A.U., arbitrary units.

induced substates in single-channel measurements (21). In other studies, full conductances were recorded (22, 23).

We addressed the presence of RyR1–FKBP12 complex by incubating membrane isolates for 30 min with 5 μM FKBP12 before addition to the cis bilayer chamber (23). We found that treatment with FKBP12 did not significantly alter channel open probability at 2 μM cytosolic of RyR1–WT ($P_o = 0.07 \pm 0.02$ and 0.11 ± 0.02 with and without FKBP12, respectively, $n = 8–9$)

and RyR1–E3893Q/E3967Q ($P_o = 0.022 \pm 0.011$ and 0.030 ± 0.019 with and without FKBP12, respectively, $n = 6–7$).

RyR1 is activated by ATP and caffeine and inhibited by Mg^{2+} (3). Single-channel traces (Fig. 5A) and averaged -fold changes of P_o values (Fig. 5B) show that at 0.01 μM cytosolic Ca^{2+} , the initial addition of 5 mM caffeine increased RyR1–WT, RyR1–E3893Q/E3967Q, and E3893V/E3967V channel activities from their low P_o values (Table 1). The addition of caffeine signifi-

Activation of RyR1 by Ca²⁺

Table 1

Properties of WT and variant channels

ND, not determined. Numbers in parentheses indicate the number of independent determinations.

	Immunoblot intensity		Caffeine-induced Ca ²⁺ release		Single-channel properties			
	% WT ^a	% WT ^b	P _o at 0.01 μM Ca ²⁺	P _o at 2 μM Ca ²⁺	γ ^{K+}	P ^S	P ^{Ca} /P ^K	
WT	100	100	0.0003 ± 0.0001 (7)	0.10 ± 0.03 (10)	766 ± 11 (12) ^f	6.6 ± 0.2 (8) ^c		
E3893Q	540 ± 218 (9)	119.0 ± 7.2 (4)	0.0019 ± 0.0008 (4)	0.0015 ± 0.0003 (4)	810 ± 22 (4)	ND		
E3893V	772 ± 265 (9)	101.2 ± 11.2 (3)	0.0009 ± 0.0007 (4)	0.0007 ± 0.0005 (4) ^d	809 ± 13 (4)	ND		
E3967Q	298 ± 76 (8)	77.6 ± 9.9 (4)	0.0005 ± 0.0003 (3)	0.0017 ± 0.0011 (4)	780 ± 10 (4)	ND		
E3967V	494 ± 212 (9)	46.5 ± 5.9 (5) ^e	0.0005 ± 0.0003 (4)	0.0011 ± 0.0004 (4)	746 ± 18 (4)	ND		
E3893Q/E3967Q	207 ± 70 (10)	105.6 ± 11.0 (4)	0.020 ± 0.008 (10)	0.016 ± 0.006 (10)	790 ± 7 (5)	6.2 ± 0.3 (4)		
E3893V/E3967V	728 ± 372 (9)	48.9 ± 11.2 (4)	0.0004 ± 0.0002 (7)	0.0004 ± 0.0001 (8) ^{d,f}	774 ± 24 (3)	ND		
T5001A	103 ± 40 (5)	73.5 ± 11.5 (8)	0.0004 ± 0.0003 (3)	0.009 ± 0.007 (9)	788 ± 14 (4)	6.1 ± 0.3 (4)		

^a Intensities of RyR1 variant bands on immunoblots were normalized to RyR1-WT intensities.

^b Numbers of variant cells responding to 8 mM caffeine were normalized to WT cells showing a caffeine response; for each determination, 30–50 cells were examined.

^c From Xu *et al.* (30).

^d *p* < 0.05 compared with WT by Kruskal–Wallis one-way ANOVA followed by Dunn’s method.

^e *p* < 0.05 compared with E3893Q by Kruskal–Wallis one-way ANOVA followed by Dunn’s method.

^f *p* < 0.05 compared with E3893Q/E3967Q by Kruskal–Wallis one-way ANOVA followed by Dunn’s method.

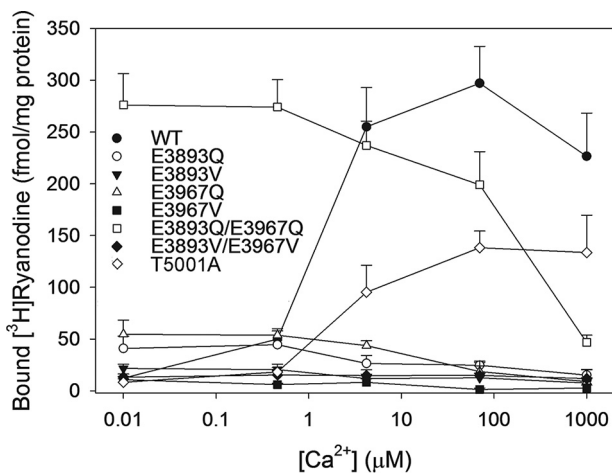


Figure 3. Effects of Ca²⁺ on [³H]ryanodine binding to RyR1-WT and variants. Specific [³H]ryanodine binding to RyR1-WT and RyR1-E3893Q, -E3893V, -E3967Q, -E3967V, -E3893Q/E3967Q, -E3893V/E3967V, and -T5001A variants was determined as described under “Experimental procedures” in the absence or presence of 10 μM unlabeled ryanodine in 0.25 M KCl, 20 mM imidazole, pH 7.0, containing 3 nM [³H]ryanodine, protease inhibitors, and the indicated concentrations of free Ca²⁺. Data are the mean ± S.E. (error bars) of 4–7 experiments.

cantly increased channel activity using Student’s *t* test. The subsequent addition of 2 mM ATP further increased channel activities (Fig. 5A). One-way but not two-way ANOVA (except for WT) indicated significant increases of P_o after the addition of 5 mM caffeine and 2 mM ATP compared with control (Fig. 5B). RyR1-E3893Q/E3967Q was inhibited ~10-fold by 0.25 mM Mg²⁺ (Fig. 5, C and D), whereas inhibition of RyR1-WT and RyR1-E3893V/E3967V was not determined due to very low open channel probability. The results suggest that RyR1-E3893Q/E3967Q and E3893V/E3967V maintained the ability of WT to be activated by caffeine and ATP and of E3893Q/E3967Q to be inhibited by Mg²⁺.

Single RyR1-WT and RyR1-E3893Q/E3967Q, -E3893V/E3967V, and -T5001A variant channel activities were also determined under conditions comparable with those of open RyR1 channels in the presence of the three channel activators Ca²⁺, ATP, and caffeine (9). The addition of 2 mM ATP and 5 mM caffeine to cytosolic 30 μM Ca²⁺ raised single-channel activities of WT and variant channels (Fig. 6A). Averaged P_o values of RyR1-WT increased 2.9-fold from 0.20 to 0.57, those

of RyR1-E3893Q/E3967Q increased 70-fold from 0.003 to 0.207, those of RyR1-E3893V/E3967V increased 46-fold from 0.0003 to 0.014, and those of RyR1-T5001A increased 11-fold from 0.029 to 0.32 (Fig. 6B), confirming that all three variants retained ATP/caffeine activation.

Discussion

Three amino acid residues that directly interact with Ca²⁺ in the high-affinity Ca²⁺-binding site were mutated and characterized. The results suggest that the high-affinity Ca²⁺-binding site plays a critical role in Ca²⁺-dependent activation of RyR1. Neutralization of negatively charged Glu-3893 and Glu-3967 resulted in loss of Ca²⁺-dependent activation of RyR1. Loss of activation appeared to be specific because other regulatory mechanisms, such as RyR1 ion permeation, inhibition by Mg²⁺ and elevated levels of Ca²⁺, and activation by ATP and caffeine, were maintained in single-channel measurements. RyR1-T5001A differentially affected RyR1 Ca²⁺ activation by shifting the Ca²⁺ activation/inactivation curve rightward relative to WT in single-channel measurements. Computational analysis using cryo-EM densities determined the structure of the Ca²⁺-binding sites of nominally Ca²⁺-free and Ca²⁺/ATP/caffeine-activated variant channels.

The Ca²⁺-binding site is located in the large cytoplasmic side of RyR1 ~70 nm from the transmembrane effector channel sites. This suggests that transition from the nominally Ca²⁺-free closed to the Ca²⁺-activated open channel involves additional sites. RyR1-E4032A mutation outside the Ca²⁺-binding site (9) exhibited a reduced Ca²⁺-dependent channel activity in lipid bilayers (24) and depolarization-induced Ca²⁺ transients in myotubes (25). Activation of the RyR1-Δ183–4006 deletion variant by micromolar Ca²⁺ suggested a Ca²⁺-activation site different from the one identified by cryo-EM (26). Other regions shown to be involved in activation and inactivation of RyR1 by Ca²⁺ include residues in the transmembrane helix S2 (27), S4–S5 linker (28, 29), and pore-lining S6 helix of skeletal muscle and cardiac-muscle RyR isoforms (30, 31).

Ca²⁺-induced Ca²⁺ release has been suggested to contribute little to the depolarization-induced Ca²⁺ release in adult mammalian skeletal muscle (15, 16). This raises the question of the physiological significance of Ca²⁺ activation of RyR1 seen with isolated RyR1s. We reported that the RyR1-G4941K mutation

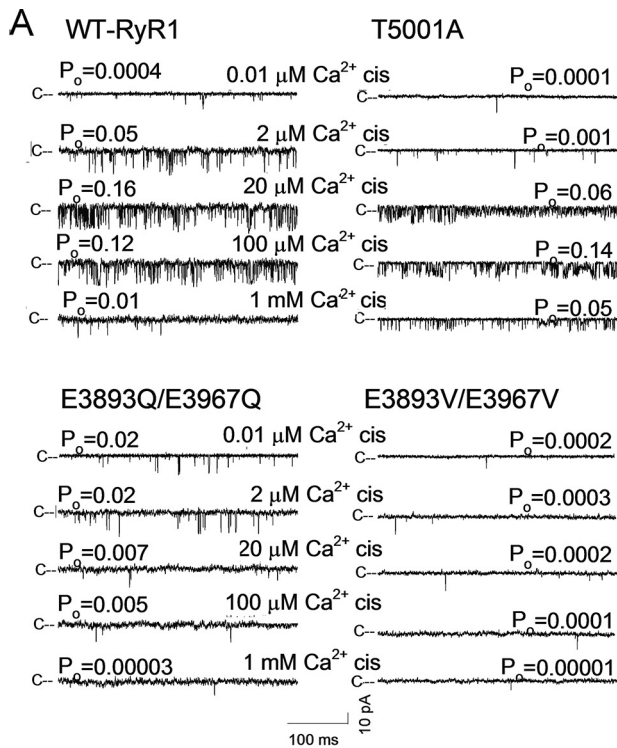


Figure 4. Single-channel measurements of RyR1-WT and RyR1-T5001A, E3893Q/E3967Q, and E3893V/E3967V variants. *A*, single-channel currents were recorded at a holding potential of -20 mV as downward deflections from the closed state ($c-$) in symmetrical 0.25 M KCl with 2 μ M SR luminal Ca^{2+} and the indicated cytosolic Ca^{2+} concentrations. *B*, Ca^{2+} dependence of RyR1-WT and RyR1-T5001A and -E3893Q/E3967Q variant channel open probabilities. Data are the mean \pm S.E. (error bars) of 3–21 recordings.

in the pore-lining S6 helix increased RyR1 sensitivity to luminal Ca^{2+} (30). This suggested that luminal Ca^{2+} activates RyR1 by accessing the cytosolic Ca^{2+} -binding site in the open channel. Thus an intriguing possibility is that in skeletal muscle, voltage-dependent activation of Cav1.1 renders the Ca^{2+} -binding site accessible to SR luminal Ca^{2+} passing through the channel and amplifies depolarization-induced Ca^{2+} release via a Ca^{2+} -induced Ca^{2+} release mechanism.

Murayama *et al.* (32) reported results using RyR2 variants that correspond to RyR1-E3893 and -E3967 while this paper was under revision. Alanine substitution of glutamates caused loss of [³H]ryanodine binding to RyR2-E3847A and -E3921A. Decreasing size but not charge resulted in minimal [³H]ryano-

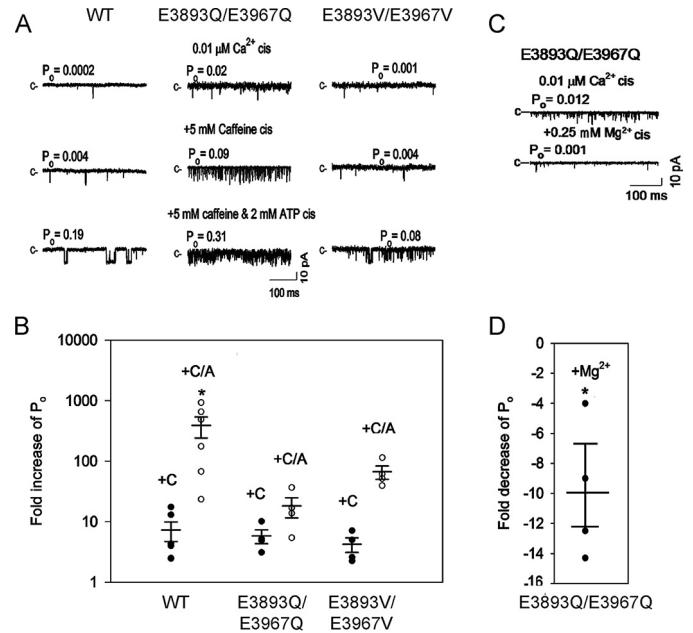


Figure 5. Effects of caffeine, ATP, and Mg^{2+} on RyR1-WT and E3893Q/E3967Q and E3893V/E3967V variant channel open probabilities in the absence of cytosolic Ca^{2+} . *A* and *C*, representative single-channel currents are shown at -20 mV as downward deflections from the closed state ($c-$) in symmetrical 0.25 M KCl with 2 μ M SR luminal Ca^{2+} , 0.01 μ M cytosolic Ca^{2+} , and the indicated sequential additions of caffeine and ATP (*A*) and Mg^{2+} (*C*). *B*, -fold increase of normalized P_o after the addition of caffeine (\bullet , $+C$) and 5 mM caffeine plus 2 mM ATP (\circ , $+C/A$). *D*, -fold decrease of P_o after the addition of 0.25 mM Mg^{2+} . *B* and *D*, data are the mean \pm S.E. (error bars) of 4–6 experiments. *, $p < 0.05$ compared with respective controls by two-way ANOVA followed by the Holm–Sidak method (*B*) and Student's *t* test (*D*).

dine binding to RyR2-E3847D, whereas RyR2-E3921D had a Ca^{2+} -binding profile similar to RyR2-WT. The results suggest that, as in RyR1, the corresponding Ca^{2+} -binding site of RyR2 has a critical role in the regulation by Ca^{2+} .

Replacement of negatively charged glutamate residues Glu-3893 and Glu-3967 with glutamine and valine resulted in loss of Ca^{2+} -dependent activation of RyR1. Glu, Gln, and Val residues have a similar residue volume of 140, 147, and 139 \AA^3 , respectively (17), suggesting that electrostatic interactions between Ca^{2+} and Glu residues contributed to transducing the functional effects of Ca^{2+} .

We determined single-channel and structural properties of the Ca^{2+} -binding site of RyR1-T5001A, -E3893Q/E3967Q, and -E3893V/E3967V variants under conditions similar to those reported by des Georges *et al.* (9). Single-channel activities and structure of the purified RyR1-FKBP12.6 (Calstabin2) complex were determined in the absence of Ca^{2+} , the presence of Ca^{2+} , the presence of ATP/caffeine, and the presence of Ca^{2+} /ATP/caffeine (9). Cryo-EM data sets were divided into four classes in an attempt to account for conformational heterogeneity. Ca^{2+} or ATP/caffeine alone resulted in constricted closed-pore conformations comparable with the Ca^{2+} -free closed states, even though a partial opening of channels was observed in the presence of 30 μ M cytosolic Ca^{2+} or 2 mM ATP/ 5 mM caffeine in lipid bilayer studies. In contrast, in the combined presence of the three channel activators Ca^{2+} , ATP, and caffeine, channels were nearly fully activated in single-channel recordings. Analysis of cryo-EM micrographs of Ca^{2+} /ATP/caffeine-activated

Activation of RyR1 by Ca^{2+}

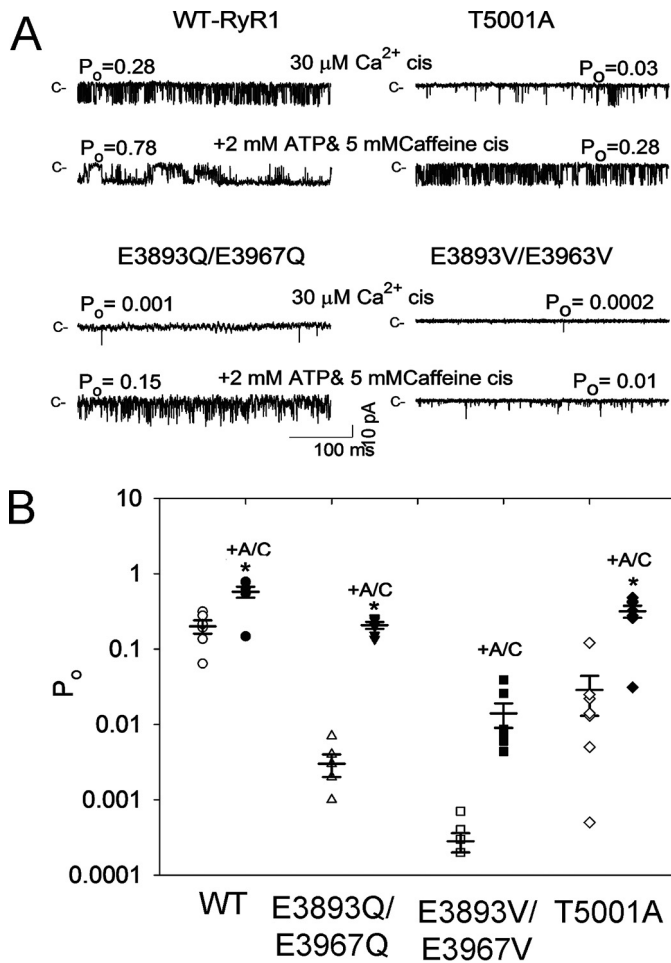


Figure 6. Effects of caffeine and ATP on RyR1-WT and RyR1-E3893Q/E3967Q, E3893V/E3967V, and T5001A variant channel open probabilities in presence of cytosolic Ca^{2+} . A, representative single-channel currents are shown at -20 mV as downward deflections from the closed state (c-) in symmetrical 0.25 M KCl. Luminal Ca^{2+} was $2 \mu M$. Free cytosolic Ca^{2+} was $30 \mu M$ (top traces) and $5 \mu M$ (as described under "Experimental procedures") after the addition of 5 mM caffeine and 2 mM ATP (+A/C) (bottom traces). B, fold increase of P_o after the addition of 5 mM caffeine plus 2 mM ATP. Data are the mean \pm S.E. (error bars) of six recordings. *, $p < 0.05$ compared with respective controls by two-way ANOVA followed by the Holm-Sidak method.

channels yielded two conformations with a dilated pore (class 1 and 2, PDB code 5TAL) and two with a constricted pore (class 3 and 4, PDB code 5TAQ), which suggested an equal number of open and closed channels. The data suggested that Ca^{2+} or ATP/caffeine alone primed RyR1 to open in the presence of the three channel activators (9). An alternative explanation was that in the presence of Ca^{2+} or ATP/caffeine, the number of open channels was too low to be scored as a separate class. In the combined presence of the three channel activators, the number of open channels was proposed to increase, as the equilibrium of channel openings/closings shifted toward the open state(s) (see Fig. S5 of des Georges et al. (9)).

In our single-channel studies, membrane-bound RyR1s were incorporated into lipid bilayers. Fig. 7 shows the structure of the Ca^{2+} -binding site of RyR1-WT and the *in silico* structures of RyR1-T5001A, -E3893Q/E3967Q, and -E3893V/E3967V variants. Low P_o values and closely related Ca^{2+} -binding structures were obtained for nominally Ca^{2+} -free RyR1-WT and RyR1-E3893V/E3967V and -T5001A variants. A weak interaction

between the Gln-3893 carboxamide group and Thr-5001 carbonyl oxygen may have contributed to elevated P_o of RyR1-E3893Q/E3967Q compared with WT and the two other variants (Fig. 7 and Table 2). The relative high P_o values of RyR1-E3893Q/E3967Q compared with WT and single E3893Q and E3967Q variants also suggested the presence of distinct structural changes among the single- and double-site RyR1-E3893Q and -E3967Q variants.

In the closed RyR1-WT channel in the presence of the three activating ligands Ca^{2+} , ATP, and caffeine, Ca^{2+} strongly interacted with Glu-3893 and Glu-3967 carboxyl oxygens and Thr-5001 carbonyl oxygen and weakly with Glu-3893 carbonyl oxygen (Fig. 7 and Table 2). Small rearrangements in the interaction of Ca^{2+} with the three amino acid residues, including loss of weak interaction with Glu-3893 carbonyl oxygen, appeared to stabilize open WT channel states.

In RyR1-E3893V/E3967V closed- and open-channel structures, loss of a strong interaction between Ca^{2+} and Val resulted in a profound decrease of channel activity, reducing $P_o = 0.57$ of WT to 0.014 for RyR1-E3893V/E3967V, which suggested a shift of the equilibrium of channel opening/closing toward the closed state(s). In the RyR1-E3893Q/E3967Q closed-channel structure, Ca^{2+} ceased to interact with the Gln carboxamides. However, in contrast to E3893V/E3967V, a strong interaction with Gln carboxamide oxygens was maintained in the open-channel states. Additionally, hydrogen bonds between three pairs of amino acid residues in the closed-channel state and one pair in the open-channel state were predicted (Fig. 7 and Table 2). We suggest that the additional interactions in RyR1-E3893Q/E3967Q stabilized the open state(s), decreasing $P_o = 0.57$ of WT to 0.21 for RyR1-E3893Q/E3967Q rather than to 0.014 for RyR1-E3893V/E3967V (Fig. 6B, +A/C). Removal of the hydroxyl group and a change in side-chain volume of RyR1-T5001A did not noticeably alter the open and closed Ca^{2+} -binding structures compared with WT. A shift of the Ca^{2+} activation/inactivation curve rightward from WT indicated that the T5001A mutation caused secondary structural changes in the presence of the three activating ligands Ca^{2+} , ATP, and caffeine. Together, the results suggest that electrostatic interactions between Ca^{2+} and glutamate residues of the RyR1 Ca^{2+} -binding site have a major role in transducing the functional effects of Ca^{2+} in RyR1.

In conclusion, our studies show that the removal of negative charges in a RyR1 Ca^{2+} -binding site impairs activation of RyR1 by physiological concentrations of Ca^{2+} and suggests loss of binding to or reduced Ca^{2+} affinity of the site. Ca^{2+} binding to inhibitory sites is expected to interfere with any low-affinity Ca^{2+} activation of RyR1. Hence, a more detailed understanding of the mechanism(s) resulting in dysfunctional Ca^{2+} activation may depend on identifying and eliminating low-affinity RyR1 Ca^{2+} -inactivation sites.

Experimental procedures

Materials

[3H]Ryanodine was obtained from PerkinElmer Life Sciences, protease and phosphatase inhibitors from Sigma-Aldrich, and phospholipids from Avanti Polar Lipids.

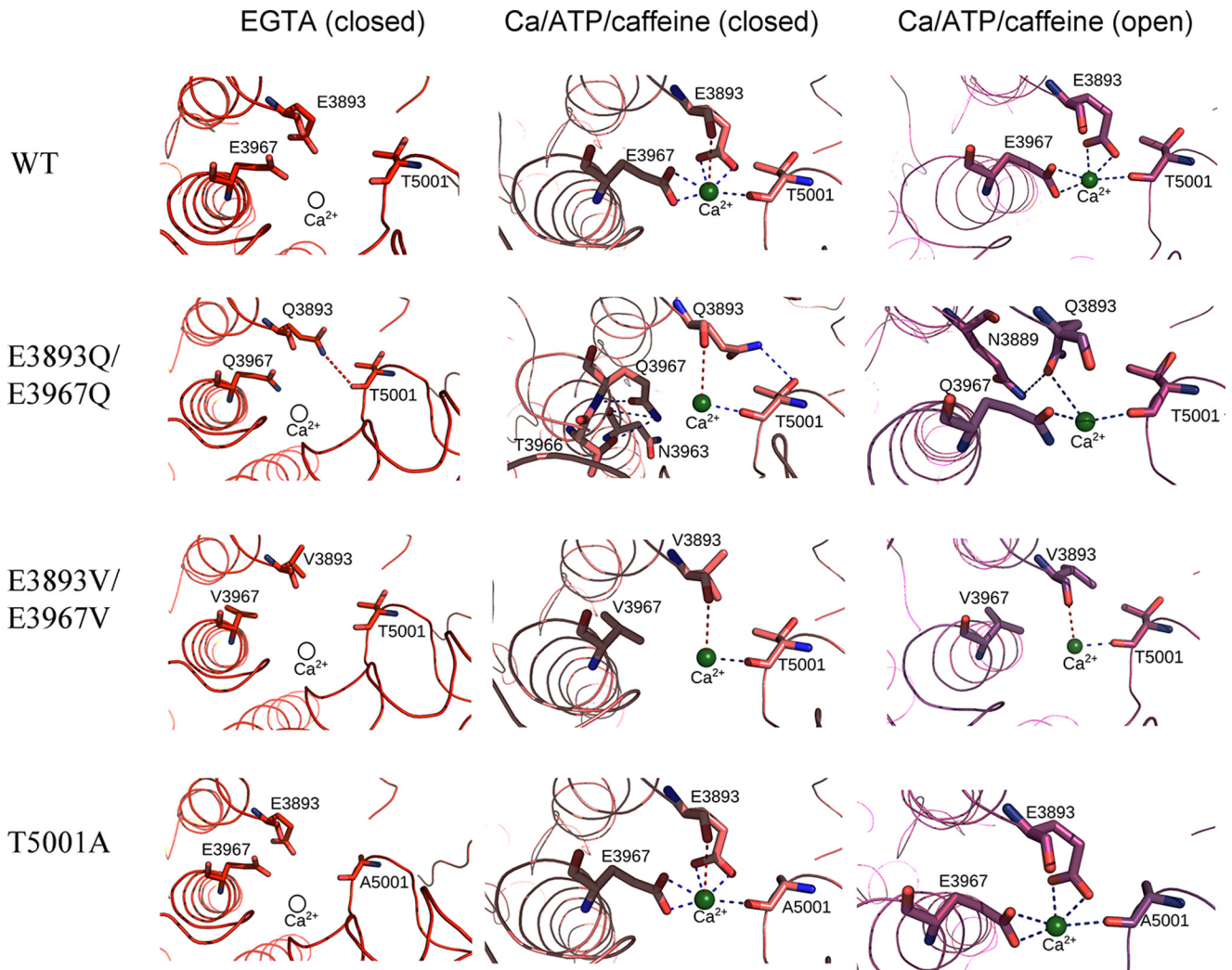


Figure 7. Interactions of Ca^{2+} with RyR1 residues in multiple functional states. Shown are the predicted interactions of Ca^{2+} with RyR1-WT and RyR1-E3893Q/E3967Q, E3893V/E3967V, and T5001A variants under nominally Ca^{2+} -free (PDB code 5TB0) and Ca^{2+} /ATP/caffeine (PDB code 5TAQ and 5TAL) conditions. Residues displaying electrostatic interactions with Ca^{2+} in the Ca^{2+} /ATP/caffeine state are depicted in a *stick representation*, and the backbone of RyR1 is shown in a *ribbon representation*. Ca^{2+} is shown as a *green sphere* in Ca^{2+} -bound states and as a *hollow sphere* in Ca^{2+} -free states. Strong electrostatic interactions ($d < 3.5$ Å) are shown as *blue dashed lines*, and weak electrostatic interactions ($3.5 < d < 4$ Å) are shown as *red dashed lines* between Ca^{2+} and RyR1 residues. Distances less than 3.5 Å formed interresidue contacts and are shown as *blue dashed lines*.

Preparation of variant channels

RyR1-E3893 and -E3967 single- and double-site variants were prepared using *Pfu* polymerase-based chain reaction, mutagenic oligonucleotides, and the QuikChange II site-directed mutagenesis kit (Agilent, Santa Clara, CA). RyR1-T5001A was prepared using a gene synthesis method (Genewiz, Inc., South Plainfield, NJ). WT and variant RyR1s were transiently expressed in HEK293 cells using jetPRIME (Polyplus, New York) according to the manufacturer's instructions. Transfected cells were harvested, and crude membrane isolates were prepared as described (33) in the presence of 1 mM GSSG.

SDS-PAGE and immunoblot analyses

Proteins in crude membrane isolates (20 μg of protein/lane) were separated using 3–12% acrylamide gradient SDS-PAGE, transferred overnight to nitrocellulose membranes, and probed using primary rabbit anti-RyR1 polyclonal antibody 6425 (30). Immunoblots were developed using peroxidase-conjugated anti-rabbit IgG, enhanced chemiluminescence, and quantified

using the Bio-Rad ChemiDoc MP Imaging System and ImageQuantTL analysis software. Intensity of RyR1 variant bands on immunoblots was normalized to RyR1-WT intensities.

Cellular Ca^{2+} release

Release of stored Ca^{2+} was determined as described (34). Briefly, Ca^{2+} transients in HEK293 cells grown on coverslips were monitored with the fluorescence Ca^{2+} indicator Fluo-4. Cellular Ca^{2+} release was induced by the addition of ~ 8 mM caffeine and monitored in individual cells using the EasyRatioPro algorithm (Photon Technology International, Lawrenceville, NJ).

[^3H]Ryanodine binding

Ryanodine binds with high specificity to RyR1 and is widely used to probe RyR activity and content (20). [^3H]Ryanodine binding was measured by incubating crude membrane isolates for 20–24 h at 24 °C in 20 mM imidazole, pH 7.0, 0.25 M KCl, 3 nM [^3H]ryanodine, and protease inhibitors at the indicated free Ca^{2+} concentrations. Nonspecific binding was determined in

Activation of RyR1 by Ca²⁺

Table 2

Interactions between Ca²⁺ and amino acids

Strong electrostatic interactions ($d < 3.5$ Å) are shown in Fig. 7 as blue dashed lines and weak electrostatic interactions ($3.5 < d < 4$ Å) are shown as red dashed lines between Ca²⁺ and RyR1 residues. Distances less than 3.5 Å formed interresidue contacts and are shown as blue dashed lines.

System	Variant	Ca ²⁺ interactions	Distance (Å)	aa interactions
EGTA (closed)	WT	Nil		Nil
	E3893Q/E3967Q	Nil		Q3893 – T5001
	E3893V/E3967V	Nil		Nil
	T5001A	Nil		Nil
Ca/ATP/caffeine (closed)	WT	E3893 (OE1)	2.4	Nil
		E3893 (OE2)	2.1	
		E3893 (O)	3.8	
		E3967 (OE1)	2.5	
		E3967 (OE2)	2.2	
	T5001 (O)	2.6		
	E3893Q/E3967Q	Q3893 (O)	3.8	Q3893 – T5001 Q3967 – T3966 Q3967 – N3963
		T5001 (O)	2.6	
	E3893V/E3967V	V3893 (O)	3.8	Nil
		T5001 (O)	2.6	
T5001A	E3893 (OE1)	2.4	Nil	
	E3893 (OE2)	2.1		
	E3893 (O)	3.8		
	E3967 (OE1)	2.5		
	E3967 (OE2)	2.2		
	A5001 (O)	2.6		
Ca/ATP/caffeine (open)	WT	E3893 (OE1)	2.3	Nil
		E3893 (OE2)	2.2	
		E3967 (OE1)	2.4	
		E3967 (OE2)	2.3	
		T5001 (O)	2.5	
	E3893Q/E3967Q	Q3893 (OE1)	3.3	Q3893 – N3889
		Q3967 (OE1)	2.3	
		T5001 (O)	2.5	
	E3893V/E3967V	V3893 (O)	3.9	Nil
		T5001 (O)	2.5	
	T5001A	E3893 (OE1)	2.3	Nil
		E3893 (OE2)	2.2	
		E3967 (OE1)	2.4	
		E3967 (OE2)	2.3	
		A5001 (O)	2.5	

the presence of 10 μM unlabeled ryanodine. Amounts of bound [³H]ryanodine were determined using a filtration assay (30).

Single-channel recordings

Membrane isolates were added to the cis (cytosolic) chamber of the bilayer apparatus (35). Single-channel recordings took advantage of the impermeability of RyRs to Cl[−] and high conductance of K⁺ relative to Ca²⁺. Channel activities were recorded using 0.25 M KCl, 20 mM KHEPES, pH 7.4, on both sides of the bilayer, 2 μM trans (SR luminal), and the indicated cis (cytosolic) Ca²⁺ concentrations. The trans side of the bilayer was defined as ground. Electrical signals were filtered at 2 kHz, digitized at 10 kHz, and analyzed at 50% threshold setting (35). Data acquisition and analysis of 2-min recordings were performed using commercially available software (pClamp, Axon Instruments). Channel activities were also recorded in symmetrical 0.25 M KCl solution with 10 mM Ca²⁺ in the trans bilayer chamber. The reversal potential was measured to determine Ca²⁺/K⁺ permeability ratios using a modified form of the Goldman–Hodgkin–Katz equation (35).

Computational methods

The effects of RyR1 mutations on Ca²⁺ binding were modeled by performing *in silico* amino acid substitutions at chosen positions in three RyR1 cryo-EM structures solved under different physiological conditions (PDB entries 5TB0, 5TAQ, and 5TAL) (9). The position of Ca²⁺ in the Ca²⁺-free RyR1 struc-

ture (PDB code 5TB0) was simulated by superposing the closed RyR1 structure (PDB code 5TAQ). *In silico* mutations at chosen residue positions in RyR1 structures were performed using the Mutagenesis tool in the PyMOL molecular visualization suite (36). We chose side-chain rotamers for substituted amino acids at selected positions based on backbone dependence and minimum clash score. For further refinement, side-chain optimizations were executed on mutated RyR1 structures using GROMACS version 4 (37). Optimized structures were visualized and analyzed for loss or gain of Ca²⁺ interactions with surrounding residues using PyMOL (36).

Biochemical assays and data analysis

Free Ca²⁺ concentrations were obtained by including in the solutions the appropriate amounts of Ca²⁺ and EGTA using a Ca²⁺-selective electrode. Free Ca²⁺ concentrations following the addition of 2 mM ATP (Fig. 6) were calculated using Max-Chelator and constants from Theo Schoenmakers' Chelator. Differences between samples were analyzed using SigmaPlot 11 Statistics. Comparison of two groups was determined by Student's *t* test or Mann–Whitney rank sum test (when data failed the normality test). Three sample groups or more were determined by one-way ANOVA with Tukey's test, Kruskal–Wallis one-way ANOVA on ranks followed by Dunn's method (when the normality test failed in one-way ANOVA), or two-way ANOVA using the Holm–Sidak method, where $p < 0.05$ was considered significant.

Author contributions—L. X., N. Y., and G. M. designed the experiments; L. X., J. S. C., and D. A. P. performed the experiments, V. R. C. and N. V. D. performed computational analysis of data, and N. Y. and G. M. wrote the paper. All authors reviewed the results and approved the final version of the manuscript.

References

1. Franzini-Armstrong, C., and Protasi, F. (1997) Ryanodine receptors of striated muscles: a complex channel capable of multiple interactions. *Physiol. Rev.* **77**, 699–729 [CrossRef Medline](#)
2. Lanner, J. T., Georgiou, D. K., Joshi, A. D., and Hamilton, S. L. (2010) Ryanodine receptors: structure, expression, molecular details, and function in calcium release. *Cold Spring Harb. Perspect. Biol.* **2**, a003996 [CrossRef Medline](#)
3. Meissner, G. (2017) The structural basis of ryanodine receptor ion channel function. *J. Gen. Physiol.* **149**, 1065–1089 [CrossRef Medline](#)
4. Zalk, R., Lehnart, S. E., and Marks, A. R. (2007) Modulation of the ryanodine receptor and intracellular calcium. *Annu. Rev. Biochem.* **76**, 367–385 [CrossRef Medline](#)
5. Yan, Z., Bai, X., Yan, C., Wu, J., Li, Z., Xie, T., Peng, W., Yin, C., Li, X., Scheres, S. H., Shi, Y., and Yan, N. (2015) Structure of the rabbit ryanodine receptor RyR1 at near-atomic resolution. *Nature* **517**, 50–55 [CrossRef Medline](#)
6. Zalk, R., Clarke, O. B., des Georges, A., Grassucci, R. A., Reiken, S., Mancina, F., Hendrickson, W. A., Frank, J., and Marks, A. R. (2015) Structure of a mammalian ryanodine receptor. *Nature* **517**, 44–49 [CrossRef Medline](#)
7. Peng, W., Shen, H., Wu, J., Guo, W., Pan, X., Wang, R., Chen, S. R., and Yan, N. (2016) Structural basis for the gating mechanism of the type 2 ryanodine receptor RyR2. *Science* **354**, aah5324 [CrossRef Medline](#)
8. Efremov, R. G., Leitner, A., Aebersold, R., and Raunser, S. (2015) Architecture and conformational switch mechanism of the ryanodine receptor. *Nature* **517**, 39–43 [CrossRef Medline](#)
9. des Georges, A., Clarke, O. B., Zalk, R., Yuan, Q., Condon, K. J., Grassucci, R. A., Hendrickson, W. A., Marks, A. R., and Frank, J. (2016) Structural

- basis for gating and activation of RyR1. *Cell* **167**, 145–157. [CrossRef](#) [Medline](#)
10. Samsó, M., Feng, W., Pessah, I. N., and Allen, P. D. (2009) Coordinated movement of cytoplasmic and transmembrane domains of RyR1 upon gating. *PLoS Biol.* **7**, e85 [Medline](#)
 11. Wei, R., Wang, X., Zhang, Y., Mukherjee, S., Zhang, L., Chen, Q., Huang, X., Jing, S., Liu, C., Li, S., Wang, G., Xu, Y., Zhu, S., Williams, A. J., Sun, F., and Yin, C. C. (2016) Structural insights into Ca²⁺-activated long-range allosteric channel gating of RyR1. *Cell Res.* **26**, 977–994 [CrossRef](#) [Medline](#)
 12. Bai, X. C., Yan, Z., Wu, J., Li, Z., and Yan, N. (2016) The central domain of RyR1 is the transducer for long-range allosteric gating of channel opening. *Cell Res.* **26**, 995–1006 [CrossRef](#) [Medline](#)
 13. Patterson, R. L., Boehning, D., and Snyder, S. H. (2004) Inositol 1,4,5-trisphosphate receptors as signal integrators. *Annu. Rev. Biochem.* **73**, 437–465 [CrossRef](#) [Medline](#)
 14. Schneider, M. F., and Chandler, W. K. (1973) Voltage dependent charge movement in skeletal muscle: a possible step in excitation-contraction coupling. *Nature* **242**, 244–246 [CrossRef](#) [Medline](#)
 15. Endo, M. (2009) Calcium-induced calcium release in skeletal muscle. *Physiol. Rev.* **89**, 1153–1176 [CrossRef](#) [Medline](#)
 16. Ríos, E. (2018) Calcium-induced release of calcium in muscle: 50 years of work and the emerging consensus. *J. Gen. Physiol.* **150**, 521–537 [Medline](#)
 17. Tsai, J., Taylor, R., Chothia, C., and Gerstein, M. (1999) The packing density in proteins: standard radii and volumes. *J. Mol. Biol.* **290**, 253–266 [CrossRef](#) [Medline](#)
 18. Rousseau, E., Ladine, J., Liu, Q. Y., and Meissner, G. (1988) Activation of the Ca²⁺ release channel of skeletal muscle sarcoplasmic reticulum by caffeine and related compounds. *Arch. Biochem. Biophys.* **267**, 75–86 [CrossRef](#) [Medline](#)
 19. Smith, J. S., Coronado, R., and Meissner, G. (1985) Sarcoplasmic reticulum contains adenine nucleotide-activated calcium channels. *Nature* **316**, 446–449 [CrossRef](#) [Medline](#)
 20. Sutko, J. L., and Airey, J. A. (1996) Ryanodine receptor Ca²⁺ release channels: does diversity in form equal diversity in function? *Physiol. Rev.* **76**, 1027–1071 [CrossRef](#) [Medline](#)
 21. Brillantes, A. B., Ondrias, K., Scott, A., Kobrinsky, E., Ondriasová, E., Moschella, M. C., Jayaraman, T., Landers, M., Ehrlich, B. E., and Marks, A. R. (1994) Stabilization of calcium release channel (ryanodine receptor) function by FK506-binding protein. *Cell* **77**, 513–523 [CrossRef](#) [Medline](#)
 22. Barg, S., Copello, J. A., and Fleischer, S. (1997) Different interactions of cardiac and skeletal muscle ryanodine receptors with FK-506 binding protein isoforms. *Am. J. Physiol.* **272**, C1726–C1733 [CrossRef](#) [Medline](#)
 23. Mei, Y., Xu, L., Kramer, H. F., Tomberlin, G. H., Townsend, C., and Meissner, G. (2013) Stabilization of the skeletal muscle ryanodine receptor ion channel-FKBP12 complex by the 1,4-benzothiazepine derivative S107. *PLoS One* **8**, e54208 [CrossRef](#) [Medline](#)
 24. Fessenden, J. D., Chen, L., Wang, Y., Paolini, C., Franzini-Armstrong, C., Allen, P. D., and Pessah, I. N. (2001) Ryanodine receptor point mutant E4032A reveals an allosteric interaction with ryanodine. *Proc. Natl. Acad. Sci. U.S.A.* **98**, 2865–2870 [CrossRef](#) [Medline](#)
 25. O'Brien, J. J., Feng, W., Allen, P. D., Chen, S. R., Pessah, I. N., and Beam, K. G. (2002) Ca²⁺ activation of RyR1 is not necessary for the initiation of skeletal-type excitation-contraction coupling. *Biophys. J.* **82**, 2428–2435 [CrossRef](#) [Medline](#)
 26. Bhat, M. B., Zhao, J., Takeshima, H., and Ma, J. (1997) Functional calcium release channel formed by the carboxyl-terminal portion of ryanodine receptor. *Biophys. J.* **73**, 1329–1336 [CrossRef](#) [Medline](#)
 27. Gomez, A. C., and Yamaguchi, N. (2014) Two regions of the ryanodine receptor calcium channel are involved in Ca²⁺-dependent inactivation. *Biochemistry* **53**, 1373–1379 [CrossRef](#) [Medline](#)
 28. Murayama, T., Kurebayashi, N., Oba, T., Oyamada, H., Oguchi, K., Sakurai, T., and Ogawa, Y. (2011) Role of amino-terminal half of the S4-S5 linker in type 1 ryanodine receptor (RyR1) channel gating. *J. Biol. Chem.* **286**, 35571–35577 [CrossRef](#) [Medline](#)
 29. Ramachandran, S., Chakraborty, A., Xu, L., Mei, Y., Samsó, M., Dokholyan, N. V., and Meissner, G. (2013) Structural determinants of skeletal muscle ryanodine receptor gating. *J. Biol. Chem.* **288**, 6154–6165 [CrossRef](#) [Medline](#)
 30. Xu, L., Mowrey, D. D., Chirasani, V. R., Wang, Y., Pasek, D. A., Dokholyan, N. V., and Meissner, G. (2018) G4941K substitution in the pore-lining S6 helix of the skeletal muscle ryanodine receptor increases RyR1 sensitivity to cytosolic and luminal Ca²⁺. *J. Biol. Chem.* **293**, 2015–2028 [CrossRef](#) [Medline](#)
 31. Sun, B., Guo, W., Tian, X., Yao, J., Zhang, L., Wang, R., and Chen, S. R. (2016) The cytoplasmic region of inner helix S6 is an important determinant of cardiac ryanodine receptor channel gating. *J. Biol. Chem.* **291**, 26024–26034 [CrossRef](#) [Medline](#)
 32. Murayama, T., Ogawa, H., Kurebayashi, N., Ohno, S., Horie, M., and Sakurai, T. (2018) A tryptophan residue in the caffeine-binding site of the ryanodine receptor regulates Ca²⁺ sensitivity. *Commun. Biol.* **1**, 98 [CrossRef](#) [Medline](#)
 33. Gao, L., Tripathy, A., Lu, X., and Meissner, G. (1997) Evidence for a role of C-terminal amino acid residues in skeletal muscle Ca²⁺ release channel (ryanodine receptor) function. *FEBS Lett.* **412**, 223–226 [CrossRef](#) [Medline](#)
 34. Wang, Y., Xu, L., Duan, H., Pasek, D. A., Eu, J. P., and Meissner, G. (2006) Knocking down type 2 but not type 1 calsequestrin reduces calcium sequestration and release in C2C12 skeletal muscle myotubes. *J. Biol. Chem.* **281**, 15572–15581 [CrossRef](#) [Medline](#)
 35. Xu, L., Wang, Y., Gillespie, D., and Meissner, G. (2006) Two rings of negative charges in the cytosolic vestibule of type-1 ryanodine receptor modulate ion fluxes. *Biophys. J.* **90**, 443–453 [CrossRef](#) [Medline](#)
 36. DeLano, W. L. (2011) *The PyMOL Molecular Graphics System*, version 1.5.0.4. Schroedinger, LLC, New York
 37. Hess, B., Kutzner, C., van der Spoel, D., and Lindahl, E. (2008) GROMACS 4: algorithms for highly efficient, load-balanced, and scalable molecular simulation. *J. Chem. Theory Comp.* **4**, 435–447 [CrossRef](#)